

# Density Functional Theory Study on Defect Behavior Related to the Bulk Lifetime of Silicon Crystals for Power Device Application

*Daiki Tsuchiya,\* Koji Sueoka, and Hidekazu Yamamoto*

Among the insulated-gate bipolar transistors (IGBTs) and PIN junction diodes, there are devices that the recombination centers, namely lifetime-control defects, are introduced into phosphorus (P) doped n-type silicon (Si) crystals by electron beam irradiation. The lifetime-control defects are considered as they form deep levels such as the vacancy–vacancy (V–V) pair and vacancy–phosphorus (V–P) pair. In the case of using Czochralski Si wafers, it is considered that some pairs of carbon (C), oxygen (O), and their complexes are believed to have a negative impact to the lifetime-control defects. In this study, density functional theory (DFT) calculations are performed to understand the formation behavior of lifetime-control defects and the formation behavior of complexes composed of C and O atoms believed to interact with lifetime-control defects. On the basis of these results, DFT calculations related to the structural change of lifetime-control defects are performed. The most important result is that instead of the interstitial carbon–substitutional carbon ( $C_i$ – $C_s$ ) pair, the interstitial  $C_i$  atom and interstitial carbon–interstitial oxygen ( $C_i$ – $O_i$ ) pair are the strong candidates to affect controllability of lifetime by interacting with V composed of lifetime-control defects.

The most serious problem is that the lifetime is extended by the structural changes of lifetime-control defects during a power supply operation.<sup>[1,2]</sup> However, the mechanism that causes the structural changes is still unknown.

Lifetime-control defects are considered as they form deep levels such as a vacancy–vacancy (V–V) pair and vacancy–phosphorus (V–P) pair.<sup>[3–7]</sup> In the case of using Czochralski (CZ) Si wafers, interstitial carbon ( $C_i$ ) atoms are formed by the reaction of substitutional carbon ( $C_s$ ) and a self-interstitial ( $I$ ), and interstitial carbon–substitutional carbon ( $C_i$ – $C_s$ ) pairs and interstitial carbon–interstitial oxygen ( $C_i$ – $O_i$ ) pairs are believed to have a negative impact to the lifetime-control defects (V–V pair and V–P pair).<sup>[8–11]</sup>  $C_i$  atom is easily expected to be a candidate to affect controllability of lifetime by interacting with V. However, it is not still clear whether  $C_i$ – $C_s$  pair and  $C_i$ – $O_i$  pair affect the lifetime controllability.

In this study, density functional theory (DFT) calculations were performed to understand 1) the formation behavior of lifetime-control defects such as V–V and V–P pairs and 2) the formation behavior of complexes composed of C and O atoms believed to interact with lifetime-control defects. On the basis of these results, we performed calculations related to the structural changes of lifetime-control defects; the interaction of the candidate complexes, found by (1) and (2), with V or P composed of lifetime-control defects. As it will be cited and compared in this paper, a number of DFT calculations have been performed for the various defects related to vacancy, phosphorous, oxygen and carbon etc in Si crystals.<sup>[5,7,11–30]</sup> However, from the viewpoint of the influence on lifetime control defects, systematic calculations have not been reported to clarify the candidates to affect the lifetime-control defects. Especially, as far as to our knowledge, the binding energies ( $E_b$ ) of  $V$ – $C_i$ – $O_i$ ,  $P$ – $C_i$ – $O_i$ ,  $V$ – $C_i$ – $C_s$ , and  $P$ – $C_i$ – $C_s$  have not been reported yet.

A notable feature of this research is that the most stable and metastable structures were obtained without omission by calculating the  $E_b$  between reactive species by considering all the possible atomic configurations in a Si 64-atom cubic

## 1. Introduction

To achieve a low-carbon society, reducing the number of loss of power devices is an urgent problem that needs to be solved. An essential factor to achieve low-loss insulated-gate bipolar transistors (IGBTs) is controlling the bulk lifetime of phosphorus (P) doped n-type silicon (Si) crystals. Among the IGBTs and PIN junction diodes, there are devices that the recombination centers, namely lifetime-control defects, are introduced into such crystals by electron beam irradiation.<sup>[1,2]</sup>

D. Tsuchiya, Prof. K. Sueoka  
Okayama Prefectural University  
111 Kuboki, Soja, Okayama 719-1197, Japan  
E-mail: cd30022h@c.oka-pu.ac.jp

Prof. H. Yamamoto  
Chiba Institute of Technology  
2-17-1 Tsudanuma, Narashino, Chiba 275-0016, Japan

 The ORCID identification number(s) for the author(s) of this article can be found under <https://doi.org/10.1002/pssa.201800615>.

DOI: 10.1002/pssa.201800615

cell.<sup>[18,19,31]</sup> This approach provided us with the reaction path to form complexes during each reaction.

## 2. Calculation Details

The DFT calculations in this study are based on a standard approach, using a local density approximation with ultrasoft pseudopotentials and plane waves as a basis set for efficiently optimizing the atomic structure.<sup>[32]</sup> A generalized gradient approximation (GGA) was used for the exchange-correlation term, and the functional form was of the Perdew-Burke-Ernzerhof (PBE) type.<sup>[33]</sup> The cutoff energy used for the plane-wave expansion was 340 eV. The Cambridge Serial Total Energy Package (CASTEP) code is used to self-consistently solve the Kohn-Sham equation under a three-dimensional periodic boundary condition.<sup>[34]</sup> The density mixing method was used to minimize the energy of the electronic system, and the Broyden-Fletcher-Goldfarb-Shanno (BFGS) structural optimization method was used to optimize atom placement.<sup>[35,36]</sup> As for the convergence condition used in the electronic-state calculation, the total energy change was less than  $5.0 \times 10^{-7}$  eV/atom, and in geometry optimization, the total energy change was less than  $5.0 \times 10^{-6}$  eV/atom, an atomic displacement less than  $5.0 \times 10^{-4}$  Å, an atomic force less than 0.01 eV Å<sup>-1</sup>, and stress in the cell less than 0.02 GPa. We carried out k-point sampling at  $2 \times 2 \times 2$  special points in a Monkhorst-Pack grid, which was sufficient to obtain converged results for the Si 64-atom supercells.<sup>[37]</sup> A Si 64-atom cubic cell with a cell size of 10.937 Å, namely a  $2 \times 2 \times 2$  supercell constructed with a conventional cell, was used. The cell was surrounded by (100), (010), and (001) planes, and each edge of the cell was along the [100], [010], and [001] directions. Three-dimensional periodic boundary conditions were set for each calculation model. A Si 216-atom cubic cell with a cell size of 16.392 Å, namely a  $3 \times 3 \times 3$  supercell constructed with a conventional cell, was also used to obtain the more reliable  $E_b$  of the most stable complexes.

In the present work, the calculation cells were kept electronically neutral. That is, only the uncharged state is considered, while the direct exchange of electrons between two reactants in the cell is automatically taken into account. The impact of charge states will be considered in the future study.

We handled the following behaviors related to the lifetime-control defects:

- 1) Formation behavior of lifetime-control defects such as V–V and V–P.
- 2) Formation behavior of complexes believed to interact with lifetime-control defects.
- 3) Structural change of lifetime-control defects.

Considering that the target region is the P doped n-type CZ-Si crystals with electron beam irradiation, some of the intrinsic point defects (vacancy V and self-interstitial I), dopant (P) atom, and impurity (C and O) atoms were introduced in a cubic cell. Total energy ( $E_{tot}$ ) of the cell was calculated on the basis of the DFT calculation. A notable feature of this

research is that we considered all possible atomic configurations in a Si 64-atom cubic cell. This brought about the most stable and metastable structures of target complexes and the formation path of stable complexes. The calculation model used in each reaction, its initial configuration, and calculation method of binding energy are described in Sections 2.1 to 2.3.

### 2.1. Formation Behavior of Lifetime-Control Defects Such As V–V and V–P

In a Si 64-atom cubic cell, there are sites (1st to 9th) from a center atom as shown in Figure 1. In the calculation, a Vor P atom was placed at the center (in red) and the other V was arranged from the 1st to 9th sites (in blue). The binding energy ( $E_b$ ) of V and V, and of V and P are calculated with Equations (1) and (2), respectively, as

$$\begin{aligned} E_b(V, V) = & \{E_{tot}[\text{Si}_{63}V_1] + E_{tot}[\text{Si}_{63}V_1]\} \\ & - \{E_{tot}[\text{Si}_{62}V_2] + E_{tot}[\text{Si}_{64}]\} \end{aligned} \quad (1)$$

$$\begin{aligned} E_b(V, P) = & \{E_{tot}[\text{Si}_{63}V_1] + E_{tot}[\text{Si}_{63}P_1]\} \\ & - \{E_{tot}[\text{Si}_{62}V_1P_1] + E_{tot}[\text{Si}_{64}]\} \end{aligned} \quad (2)$$

### 2.2. Formation Behavior of Complexes Believed to Interact With Lifetime-Control Defects

It is known that I is most stable at the [110] dumbbell (D)-site in a perfect Si crystal.<sup>[5]</sup> In the calculation for the reaction of C and I, a substitutional carbon (C<sub>s</sub>) atom was arranged around an I. By considering the symmetry of the diamond structure, there are 36 independent models as shown in Figure 2(a). In addition to these

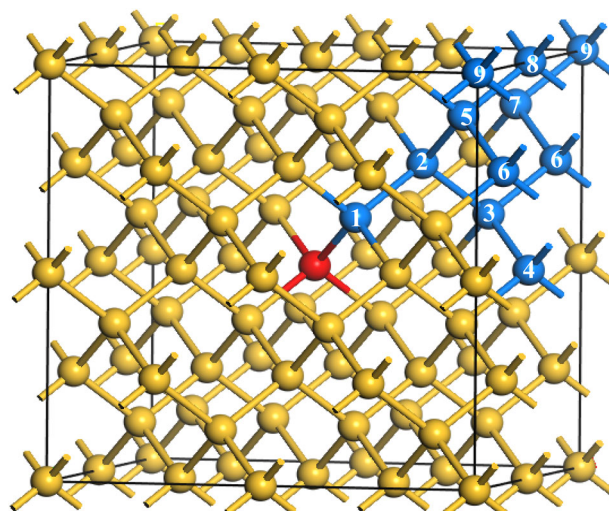
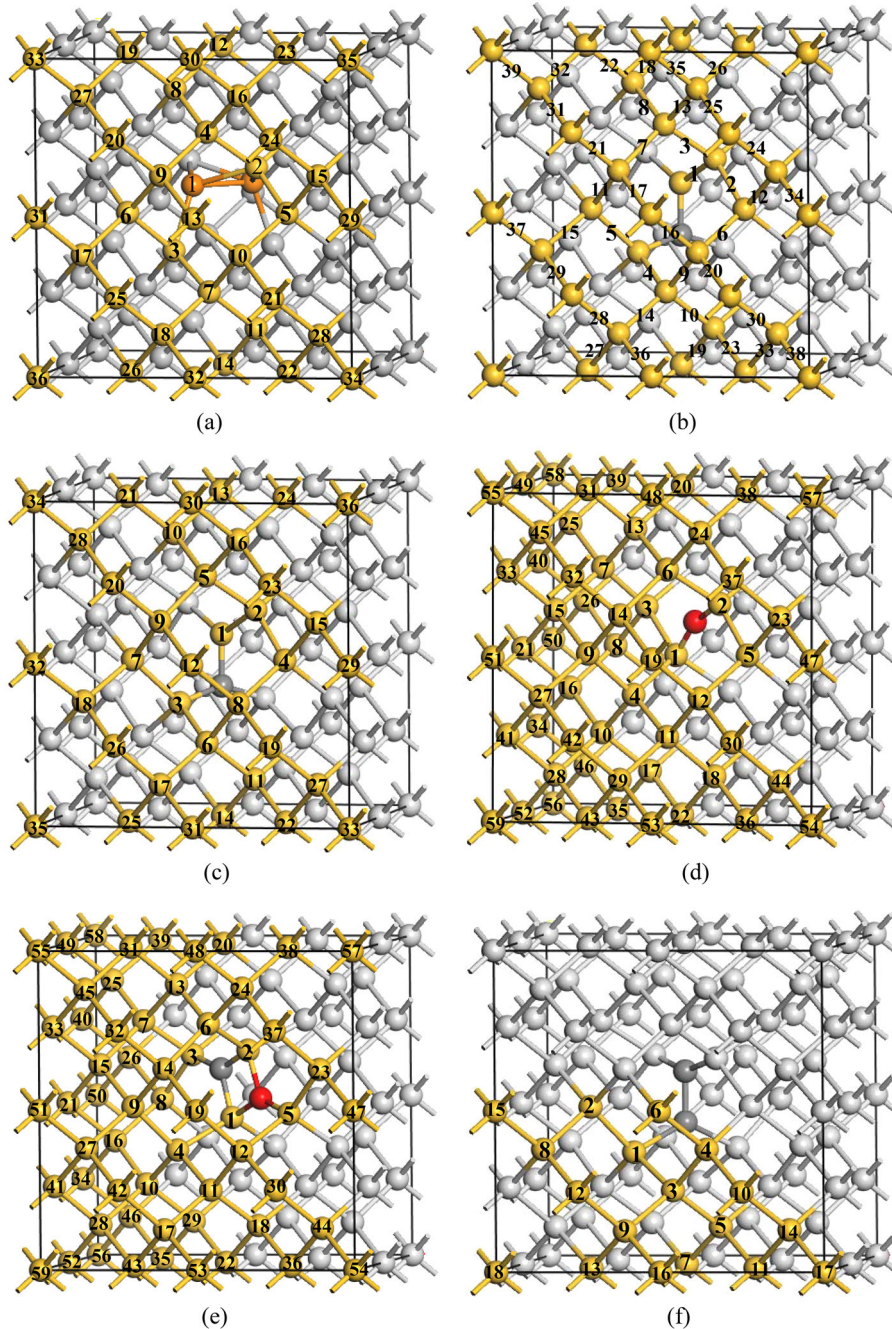


Figure 1. Si 64-atom cubic cell: 1st to 9th site (in blue) from a center atom (in red).



**Figure 2.** Initial configurations in Si 64-atom cubic cell. a) I (in orange) and site of C<sub>s</sub>; b) C<sub>i</sub> (in gray) and site of O<sub>i</sub>; c) C<sub>i</sub> (in gray) and site of C<sub>s</sub>, V, P; d) O<sub>i</sub> (in red) and site of V, P; e) C<sub>i</sub>-O<sub>i</sub> (in gray and red) and site of V, P; and f) C<sub>i</sub>-C<sub>s</sub> (in gray) and site of V, P.

models, we considered [100] D-site composed of I and C<sub>s</sub> atoms as the model No. 0. E<sub>b</sub> of I and C<sub>s</sub> was calculated with Equation (3) as

$$E_b(I, C_s) = \{E_{tot}[\text{Si}_{64}I_1] + E_{tot}[\text{Si}_{63}C_{s1}]\} - \{E_{tot}[\text{Si}_{63}I_1C_{s1}] + E_{tot}[\text{Si}_{64}]\} \quad (3)$$

Interstitial carbon (C<sub>i</sub>) and interstitial oxygen (O<sub>i</sub>) atoms are most stable at the [100] D-site and bond center

(B)-site, respectively, in a perfect Si crystal.<sup>[5,20]</sup> In the calculation for the reaction of C<sub>i</sub> and O<sub>i</sub>, an O<sub>i</sub> atom was arranged around a C<sub>i</sub> atom. By considering the symmetry of the diamond structure, there are 39 independent models as shown in Figure 2(b). E<sub>b</sub> of C<sub>i</sub> and O<sub>i</sub> was calculated with Equation (4) as

$$E_b(C_i, O_i) = \{E_{tot}[\text{Si}_{64}C_{i1}] + E_{tot}[\text{Si}_{64}O_{i1}]\} - \{E_{tot}[\text{Si}_{64}C_{i1}O_{i1}] + E_{tot}[\text{Si}_{64}]\} \quad (4)$$

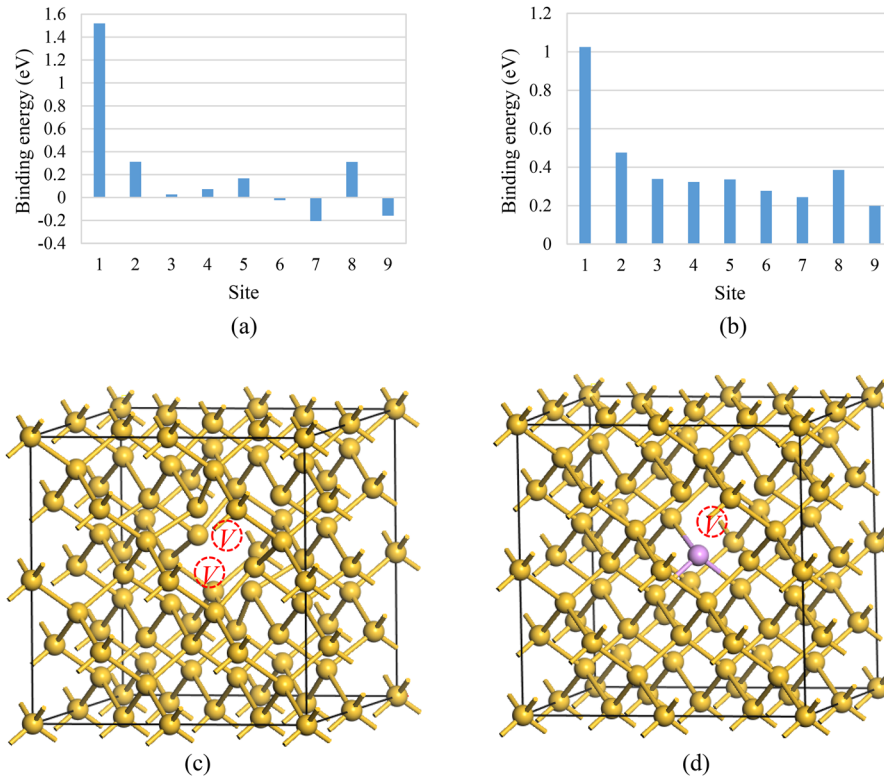


**Figure 3.** Calculation results about reaction of V and V, V and P. a) Dependence of  $E_b$  on V site from the other V; b) dependence of  $E_b$  on V site from P; c) most stable structure of V–V (No. 1); and d) most stable structure of V–P (No. 1) (purple sphere indicates P atom).

In the calculation for the reaction of  $C_i$  and  $C_s$ , a  $C_s$  atom was arranged around a  $C_i$  atom. There are 36 independent models as shown in Figure 2(c).  $E_b$  of  $C_i$  and  $C_s$  was calculated with Equation (5) as

$$E_b(C_i, C_s) = \{E_{tot}[Si_{63}C_{i1}] + E_{tot}[Si_{64}C_{s1}]\} - \{E_{tot}[Si_{63}C_{i1}C_{s1}] + E_{tot}[Si_{64}]\} \quad (5)$$

### 2.3. Structural Change of Lifetime-Control Defects

In the calculation for the reaction of V and  $C_i$  and of P and  $C_i$ , V or P was placed at the substitutional site around a  $C_i$  atom. There are 36 independent models as shown in Figure 2(c).  $E_b$  of V and  $C_i$  and of P and  $C_i$  were calculated with Equations (6) and (7) as

$$E_b(V, C_i) = \{E_{tot}[Si_{63}V_1] + E_{tot}[Si_{64}C_{i1}]\} - \{E_{tot}[Si_{63}V_1C_{i1}] + E_{tot}[Si_{64}]\} \quad (6)$$

$$E_b(P, C_i) = \{E_{tot}[Si_{63}P_1] + E_{tot}[Si_{64}C_{i1}]\} - \{E_{tot}[Si_{63}P_1C_{i1}] + E_{tot}[Si_{64}]\} \quad (7)$$

In the calculation for the reaction of V (P) and  $O_i$ , V (P) was placed at the substitutional site around an  $O_i$  atom.

There are 59 independent models as shown in Figure 2(d).  $E_b$  of V and  $O_i$  and of P and  $O_i$  are calculated with Equations (8) and (9) as

$$E_b(V, O_i) = \{E_{tot}[Si_{63}V_1] + E_{tot}[Si_{64}O_{i1}]\} - \{E_{tot}[Si_{63}V_1O_{i1}] + E_{tot}[Si_{64}]\} \quad (8)$$

$$E_b(P, O_i) = \{E_{tot}[Si_{63}P_1] + E_{tot}[Si_{64}O_{i1}]\} - \{E_{tot}[Si_{63}P_1O_{i1}] + E_{tot}[Si_{64}]\} \quad (9)$$

The  $C_i-O_i$  pair is known to be the most stable structure as shown in Figure 2(e).<sup>[11]</sup> In the calculation for the reaction of V (P) and  $C_i-O_i$ , V (P) was placed at the substitutional site around  $C_i-O_i$  pair. There are 59 independent models as shown in Figure 2(e).  $E_b$  of V and  $C_i-O_i$  and of P and  $C_i-O_i$  are calculated with Equations (10) and (11) as

$$E_b(V, C_iO_i) = \{E_{tot}[Si_{63}V_1] + E_{tot}[Si_{64}C_{i1}O_{i1}]\} - \{E_{tot}[Si_{63}V_1C_{i1}O_{i1}] + E_{tot}[Si_{64}]\} \quad (10)$$

$$E_b(P, C_iO_i) = \{E_{tot}[Si_{63}P_1] + E_{tot}[Si_{64}C_{i1}O_{i1}]\} - \{E_{tot}[Si_{63}P_1C_{i1}O_{i1}] + E_{tot}[Si_{64}]\} \quad (11)$$

The most stable  $C_i-C_s$  pair obtained is the [100] dumbbell. This structure has been demonstrated only by DFT

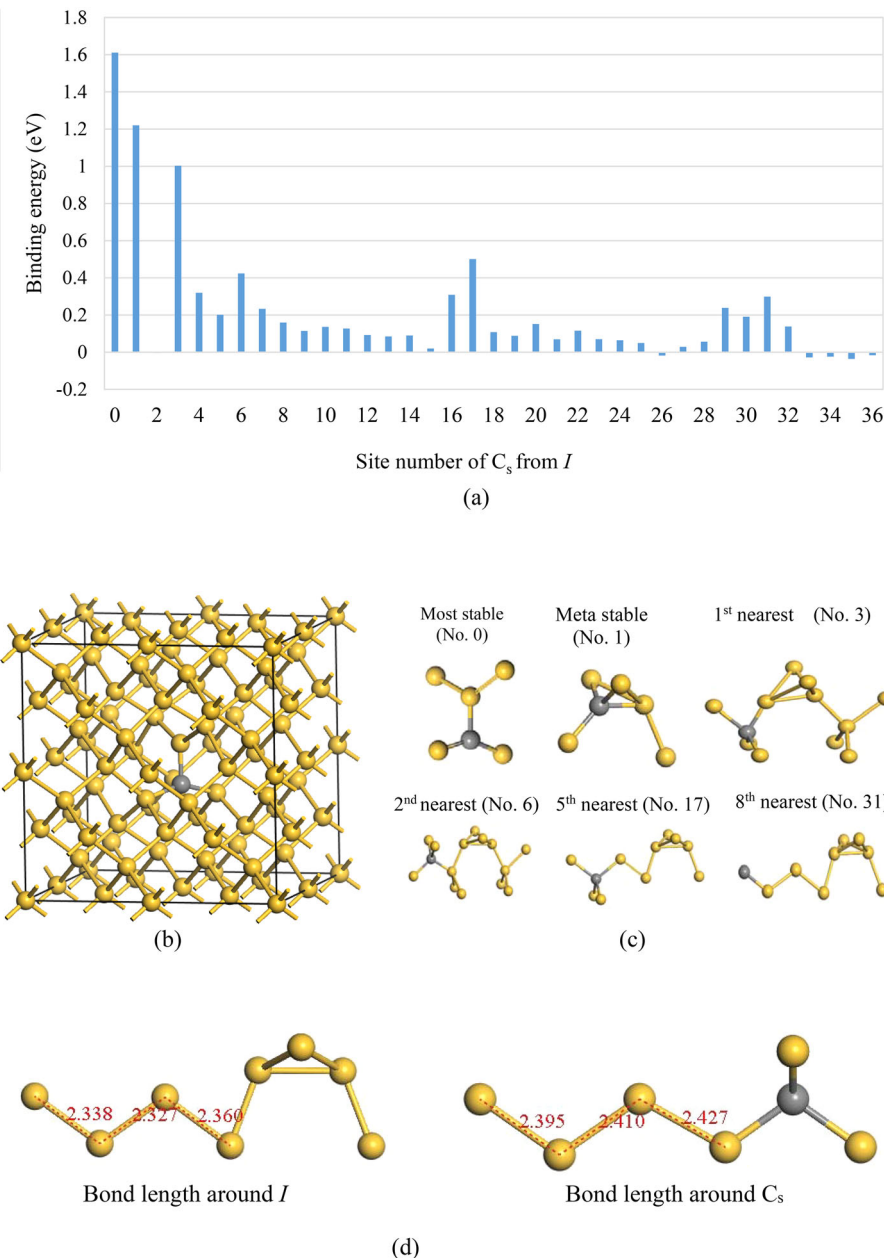


**Figure 4.** Calculation results about reaction of  $I$  and  $C_s$ . a) Dependence of  $E_b$  on the number of  $C_s$  sites from  $I$ ; b) most stable structure (No. 0) (gray sphere indicates  $C$  atom); c) most stable and metastable structures; and d) bond length around  $I$  (left) and  $C_s$  (right).

calculations.<sup>[19,21]</sup> V or P atom were placed at substitutional site around  $C_i-C_s$  pair. There are 18 independent models as shown in Figure 2(f).  $E_b$  of V and  $C_i-C_s$ , and of P and  $C_i-C_s$  are calculated with Equations (12) and (13) as

$$\begin{aligned} E_b(V, C_i C_s) = & \{E_{tot}[Si_{63}V_1] + E_{tot}[Si_{63}C_{i1}C_{s1}]\} \\ & - \{E_{tot}[Si_{62}V_1C_{i1}C_{s1}] + E_{tot}[Si_{64}]\} \end{aligned} \quad (12)$$

$$\begin{aligned} E_b(P, C_i C_s) = & \{E_{tot}[Si_{63}P_1] + E_{tot}[Si_{63}C_{i1}C_{s1}]\} \\ & - \{E_{tot}[Si_{62}P_1C_{i1}C_{s1}] + E_{tot}[Si_{64}]\} \end{aligned} \quad (13)$$

### 3. Results and Discussion

#### 3.1. Formation Behavior of Lifetime-Control Defect Such As V–V and V–P

Figure 3(a) and (b) show the calculated dependence of  $E_b$  on the number of V sites from the other V and P atom, respectively. From Figure 3(a), the most stable V–V pair (Figure 3c) is composed of a V existing at the 1st nearest neighbor site from the other V. At the 2nd neighbor site of the other V,  $E_b$  is much less than that at the 1st neighbor site. That is, the impact of a V on the other V stays in the 1st neighbor site.<sup>[7]</sup> This is due to the extinction of two dangling bonds when two vacancies

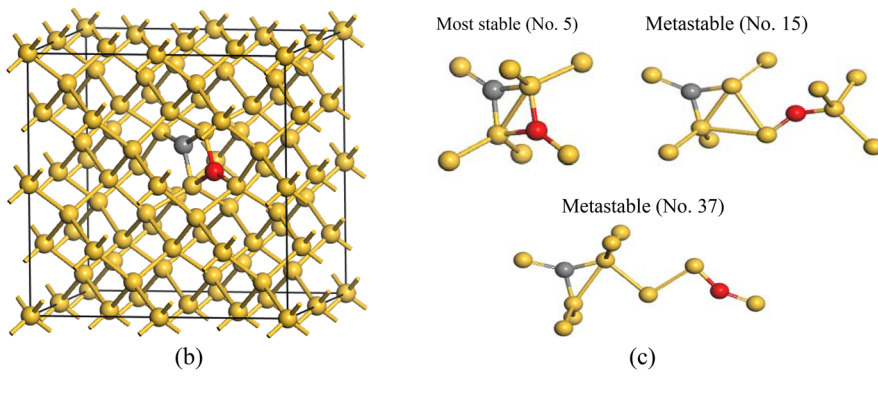
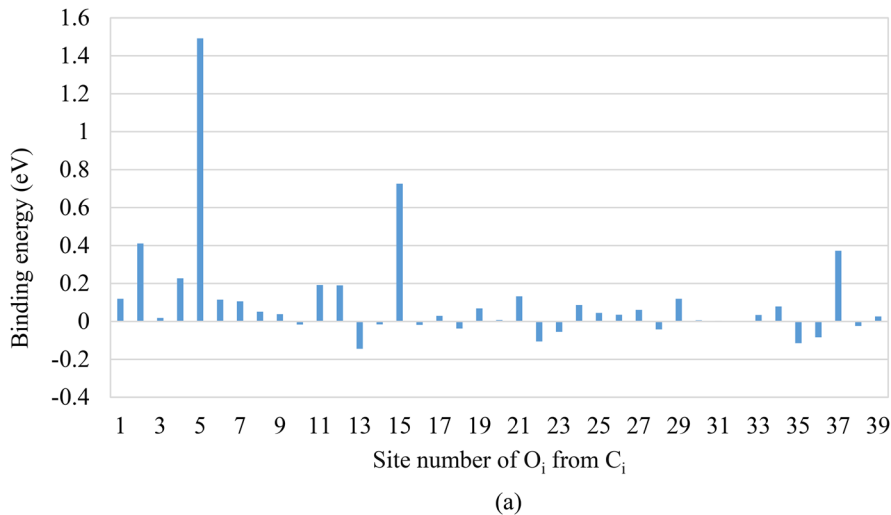


**Figure 5.** Calculation results about reaction of  $C_i$  and  $O_i$ . a) Dependence of  $E_b$  of  $C_i-O_i$  on the number of  $O_i$  sites from the  $C_i$  atom; b) most stable structure (no. 5) (gray/red sphere indicates  $C/O$  atom); c) most stable and metastable structures; and d) bond length around  $O_i$ .

form an adjacent V–V pair.  $E_b$  of V and P is also the largest when both V and P stay at the 1st neighbor site (Figure 3d). However, as shown in Figure 3(b), the value of  $E_b$  is still positive even at the farthest (9th) site ( $E_b=0.2$  eV). This result indicates that the influence of P atom on V extends beyond the cell size, which is due to the long-range electrical interaction.<sup>[18]</sup>

### 3.2. Formation Behavior of Complex Interacting Lifetime-Control Defects

#### 3.2.1. Reaction of $C_s$ and I

**Figure 4(a)** shows the calculated dependence of  $E_b$  on the number of  $C_s$  sites from I. In the reaction of I and  $C_s$ , [100]

D-site composed of I and C atoms is the most stable as shown in Figure 4(b).<sup>[5]</sup> That is, I interacts with  $C_s$ , which results in the formation of  $C_i$ . Some metastable structures are determined as shown in Figure 4(c).  $C_s$  and I are stable

**Table 1.** Bond length around  $C_i$  dumbbell.

	Direction A		Direction B	
	Connected with Si atom [Å]	Connected with C atom [Å]	Connected with Si atom [Å]	Connected with C atom [Å]
1st–2nd	2.372	2.479	2.342	2.327
2nd–5th	2.374	2.442	2.335	2.341
5th–8th	2.368	2.415	2.346	2.350

Bond length of Si-Si: 2.368 Å.

on each other's Si-Si zigzag bond. The length of Si-Si bondings in a perfect crystal is 2.368 Å. As shown in Figure 4(d), the decreased bond length around  $I$  indicates the occurrence of compressive strain, while the increased bond length around  $C_s$  atoms indicates the occurrence of tensile strain. The compensation of strains caused by  $I$  and  $C_s$  is the reason for the stable  $C_s$ - $I$  pair. In the reaction of  $I$  and  $C_s$ ,  $I$  moves to  $C_s$  atoms along the [110] direction through the metastable structures and forms  $C_i$  by the reaction of  $I + C_s \rightarrow C_i$ .

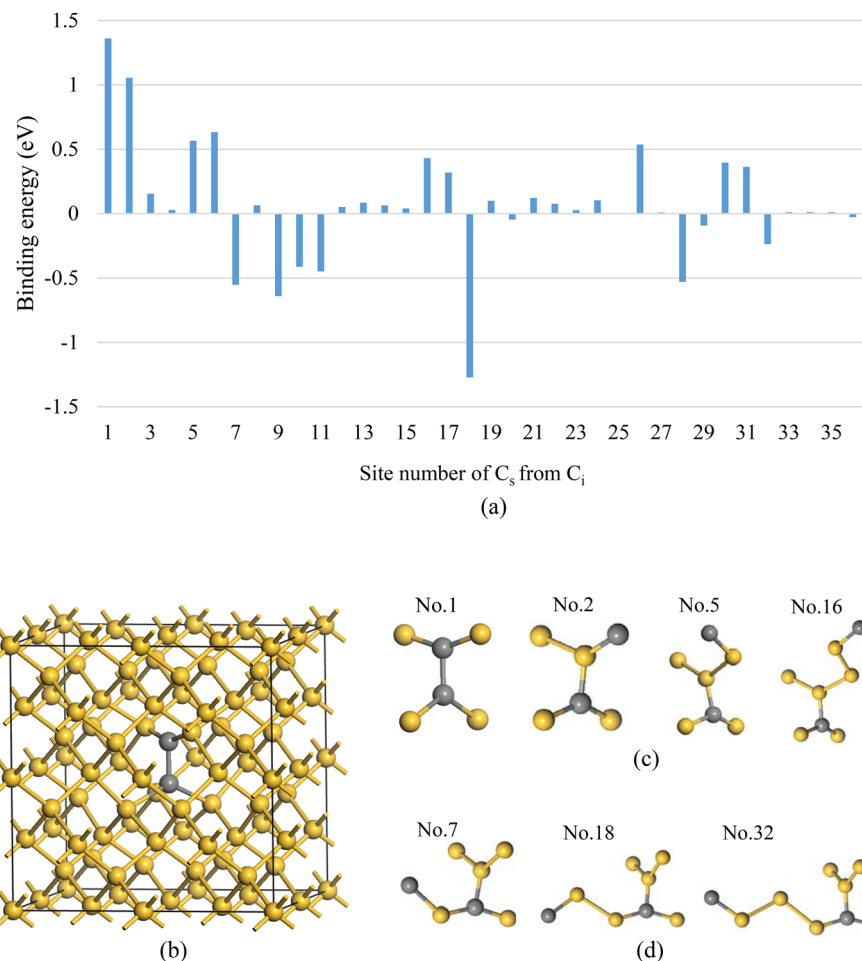
### 3.2.2. Reaction of $C_i$ and $O_i$

Figure 5(a) shows the calculated dependence of  $E_b$  of  $C_i$ - $O_i$  on the number of  $O_i$  sites from the  $C_i$  atom. As shown in Figure 5(b), both  $C_i$  and  $O_i$  atoms bond to three Si ligand atoms and share two of them. Some metastable structures are shown in Figure 5(c).  $C_i$  and  $O_i$  atoms are stable on each other's zigzag bond. As shown in Figure 5(d), compressive strain occurs on the zigzag bond including  $O_i$  atom. The calculated bond lengths of <110> zigzag bonds in the vertical direction of

[100]  $C_i$  dumbbell (direction A) and <110> zigzag bonds in the direction of angle of 45 degrees from [100]  $C_i$  dumbbell (direction B) are summarized in Table 1.  $C_i$  dumbbell causes tensile strain in the direction A and compressive strain in the direction B. By considering the local strain formed by  $C_i$  and  $O_i$  atoms,  $C_i$  and  $O_i$  approach each other from the direction A and form a  $C_i$ - $O_i$  complex with rhombic structure by the reaction of  $C_i + O_i \rightarrow C_i\text{-}O_i$ .

### 3.2.3. Reaction of $C_i$ and $C_s$

Figure 6(a) shows the calculated dependence of  $E_b$  on the number of  $C_s$  sites from the  $C_i$  atom. The determined most stable structure and some metastable structures are shown in Figure 6(b) and (c), respectively.<sup>[10]</sup> At sites No. 1,  $C_i$  and  $C_s$  atoms form [100] dumbbell, which is the most stable structure. The structure of [100] dumbbell is described as a  $C_i$ - $C_s$  defect. As described in the Section 3.2.2, the  $C_i$  atom causes compressive strain in the direction B. Therefore, the tensile strain of  $C_s$  is probably relaxed to form a  $C_i$ - $C_s$  defect.



**Figure 6.** Calculation results about reaction of  $C_i$  and  $C_s$ . a) Dependence of  $E_b$  on the number of  $C_s$  sites from the  $C_i$  atom; b) most stable structure (No. 1) (gray sphere indicates  $C$  atom); c) most stable and metastable structures; and d) unstable structures.

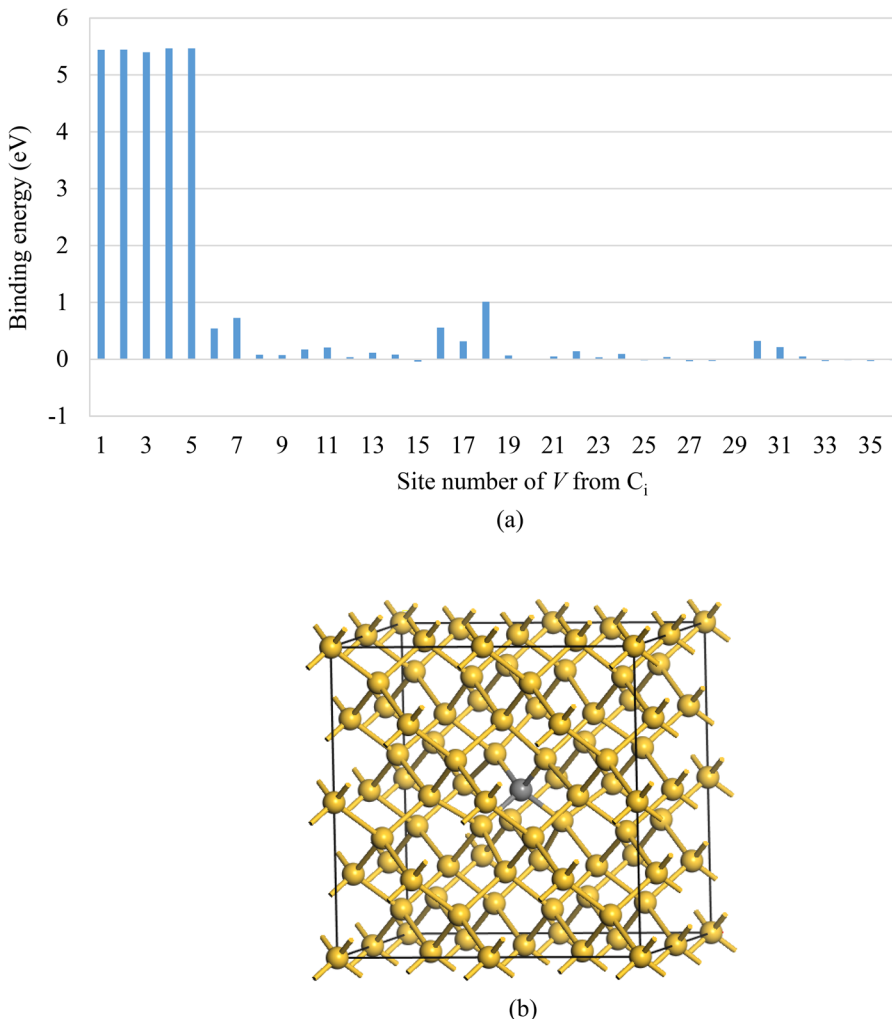


**Figure 7.** Calculation results about reaction of  $V$  and  $C_i$ . a) Dependence of  $E_b$  on the number of  $V$  sites from the  $C_i$  atom and b) most stable structure (from No. 1 to No. 5) (gray sphere indicates  $C$  atom).

### 3.3. Structural Change of Lifetime Control Defect

#### 3.3.1. Reaction of $V$ and $C_i$

**Figure 7(a)** shows the calculated dependence of  $E_b$  on the number of  $V$  sites from the  $C_i$  atom. The determined most stable structure is shown in **Figure 7(b)**.  $V$  and the  $C_i$  atom are annihilated and becomes a  $C_s$  atom, that is, a substitutional  $C_s$  atom is formed by the reaction of  $V + C_i \rightarrow C_s$ .  $V$  is stable on the Si–Si bond in the direction B of the [100]  $C_i$  dumbbell because of the compressive strain caused by  $C_i$ .  $V$  and the  $C_i$  atom should approach each other in the direction B of [100]  $C_i$  dumbbell.

#### 3.3.2. Reaction of $P$ and $C_i$

**Figure 8(a)** shows the calculated dependence of  $E_b$  on the number of  $P$  sites from the  $C_i$  atom. The most stable structure determined is shown in **Figure 8(b)**.  $P$  and  $C_i$  atoms

form the slightly distorted [100] dumbbell. Some metastable structures are shown in **Figure 8(c)**. Since  $P$  atom is slightly smaller than  $Si$  atom,  $C_i$  atom should approach to  $P$  atom in the direction B of [100]  $C_i$  dumbbell. By using the Deep Level Transient Spectroscopy method, substitutional phosphorus-interstitial carbon pair ( $P-C_i$ ) was observed at the same time when  $C_i$  disappears around room temperature.<sup>[24]</sup> The  $P-C_i$  complexes have several (at least four) metastable structures which are probably reproduced by the present calculations.<sup>[38–40]</sup>

#### 3.3.3. Reaction of $V$ and $O_i$

**Figure 9(a)** shows the calculated dependence of  $E_b$  on the number of  $V$  sites from the  $O_i$  atom.  $V$  and the  $O_i$  atom form a stable complex as shown in **Figure 9(b)**, and are stable on each other's zigzag bond. In the most stable structure, the  $O_i$  atom binds with two dangling bonds of  $V$ . The  $O_i$  atom is displaced in the direction to  $V$  as shown in **Figure 9(c)**.<sup>[20]</sup>

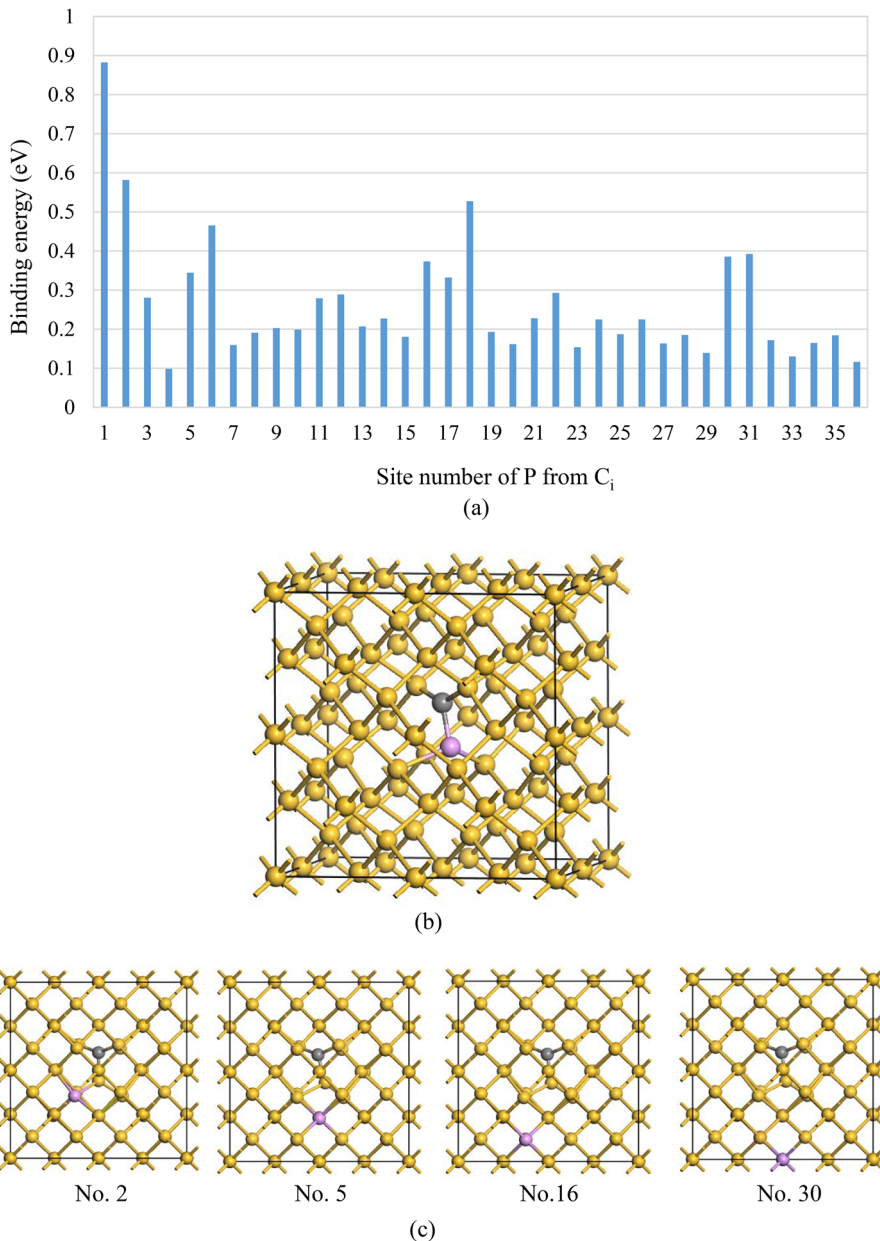


**Figure 8.** Calculation results about reaction of P and  $C_i$ . a) Dependence of  $E_b$  on the number of P sites from the  $C_i$  atom; b) most stable structure (No. 1) (gray/purple sphere indicates C/P atom); and c) several metastable structures.

### 3.3.4. Reaction of P and $O_i$

**Figure 10(a)** shows the calculated dependence of  $E_b$  on the number of P sites from the  $O_i$  atom. The most stable structure determined and some metastable structures are shown in Figure 10(b) and (c), respectively. P and  $O_i$  atoms are stable on each other's zigzag bond. Because the  $E_b$  of the P– $O_i$  pair is negative, P and  $O_i$  atoms do not bind.

### 3.3.5. Reaction of V and $C_i-O_i$

**Figure 11(a)** shows the calculated dependence of  $E_b$  on the number of Vsites from the  $C_iO_i$  pair. The most stable structure determined is shown in Figure 11(b). In the models of Vat sites No. 1, No. 4, and No.

10 shown in Figure 2(e), the  $C_i-O_i$  pair decomposes into  $C_s$  and  $O_i$  atoms. It is easily expected that V and  $C_i$  mutually annihilate, but it was also found that  $C_i$  of  $C_iO_i$  interact with Vand disappears. When V is at No. 2, the  $C_i-O_i$  pair decomposes but  $C_i$  stays at the interstitial site as shown in Figure 11(c). When V is at No. 3, Vdisappears but the structure of  $C_i-O_i$  remains. The interactive distance of V and  $C_i-O_i$  is about 4 Å.

### 3.3.6. Reaction of P and $C_i-O_i$

**Figure 12(a)** shows the calculated dependence of  $E_b$  on the number of P sites from the  $C_iO_i$  pair. The most stable structure

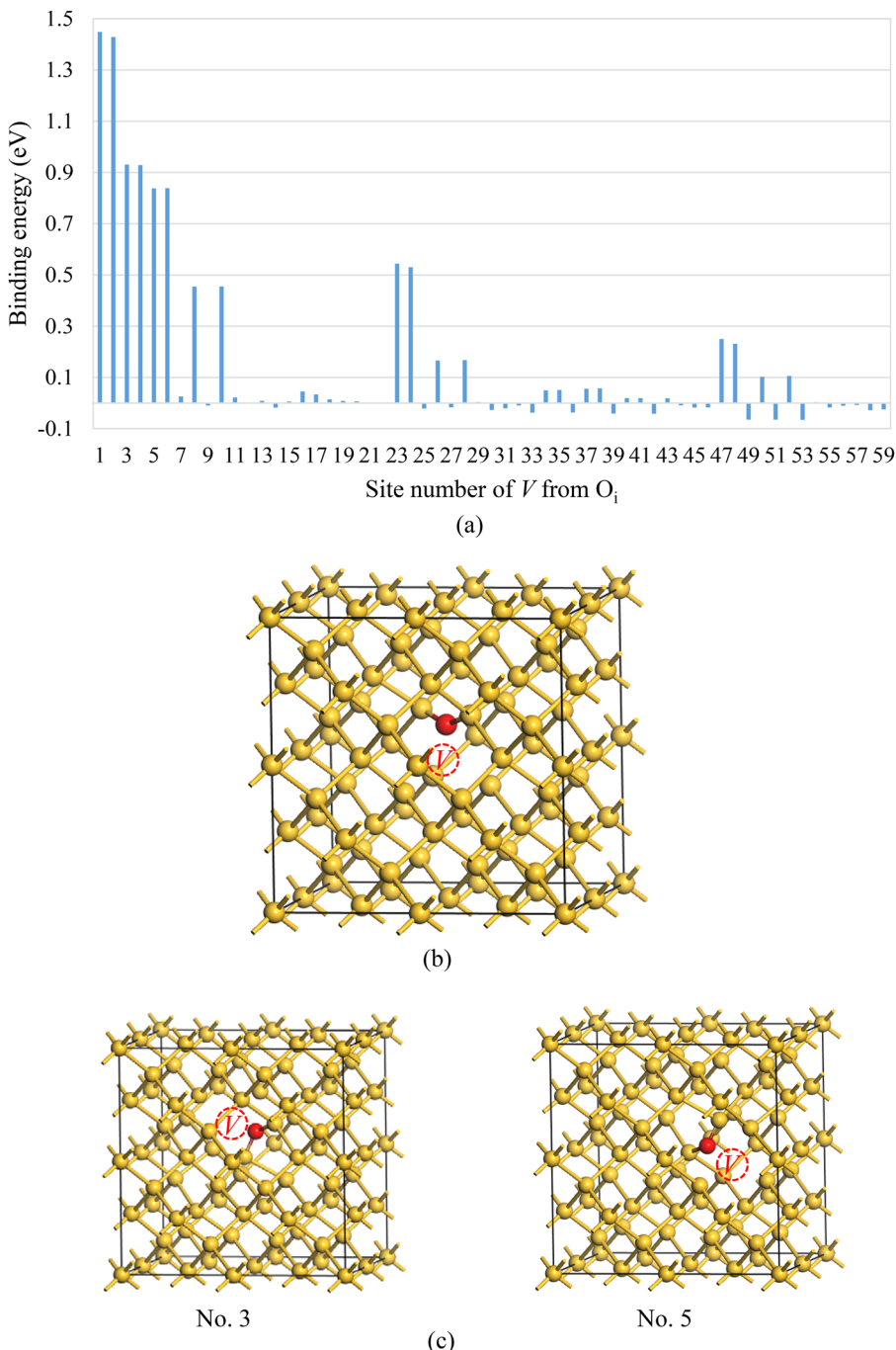


**Figure 9.** Calculation results about reaction of  $V$  and  $O_i$ . a) Dependence of  $E_b$  on the number of  $V$  sites from the  $O_i$  atom; b) most stable structure (No. 1 and No. 2) (gray/red sphere indicates  $C/O$  atom); and c) metastable structures.

determined is shown in Figure 12(b). In the most stable structure,  $P-C_iO_i$  is divided into  $P-C_i$  and  $O_i$ . The structures with negative  $E_b$  are shown in Figure 12(c).  $P$  and  $C_i-O_i$  are unstable on each other's zigzag bond as shown in Figure 12(d) without including sites No. 1 and No. 3. The combination of reactions of  $P + C_i$  and  $P + O_i$  are essential for the reaction of  $P$  and  $C_iO_i$ . In other words,  $P$  atom forms a complex with  $C_i$  atom, and not with  $O_i$  atom.

### 3.3.7. Reaction of $V$ and $C_i-C_s$

Figure 13(a) shows the calculated dependence of  $E_b$  on the number of  $V$  sites from the  $C_iC_s$  pair. The most stable  $V-C_iC_s$  pair (Figure 13b) is composed of  $V$  still existing at the 1st nearest neighbor site of  $C_iC_s$ .  $V$  and  $C_i-C_s$  pair are stable on each other's zigzag bond. There are two possible paths leading to the most stable structure: in the direction A (No. 15  $\rightarrow$  No. 8  $\rightarrow$  No. 2  $\rightarrow$  No.

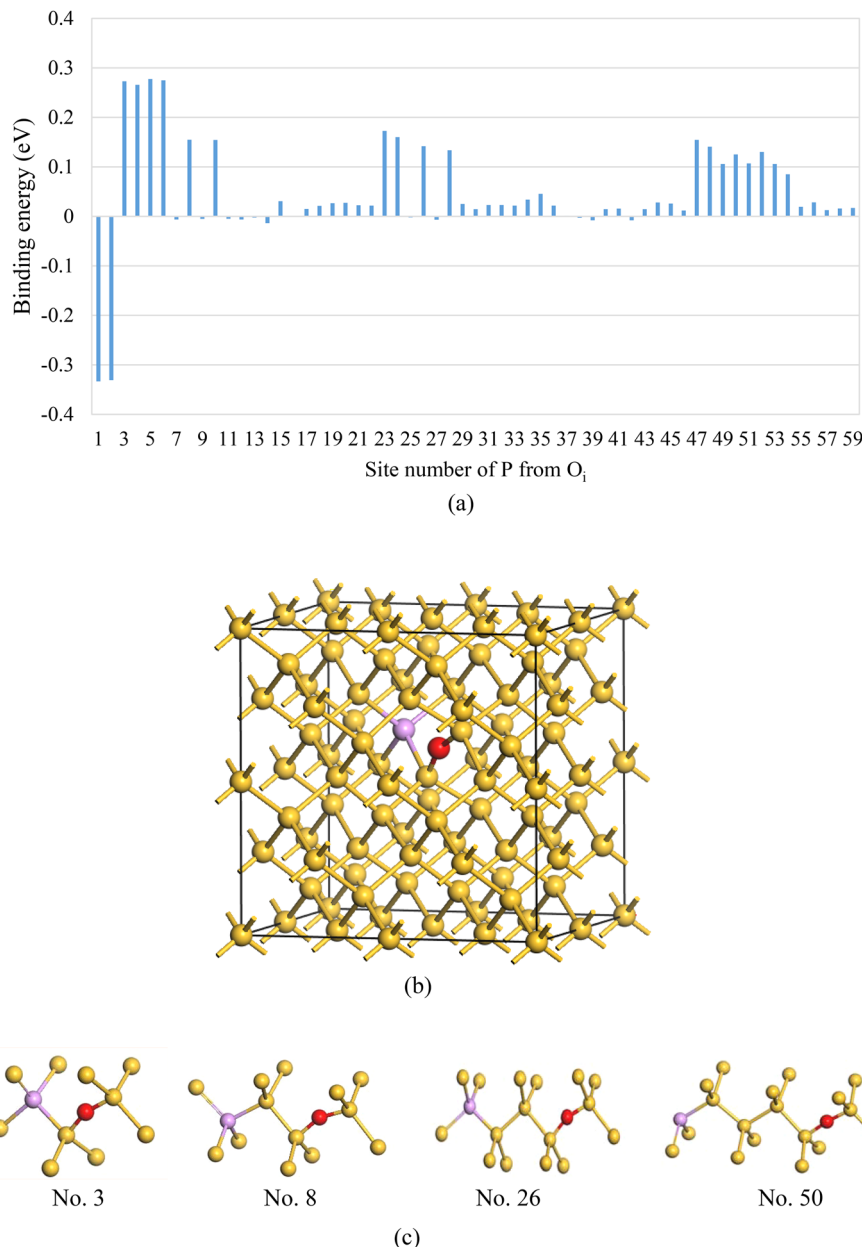


**Figure 10.** Calculation results about reaction of P and  $O_i$ . a) Dependence of  $E_b$  on the number of P sites from the  $O_i$  atom; b) most stable structure (No. 3) (red/purple sphere indicates O/P atom); and c) most stable and metastable structures.

1) and in the direction B (No. 16 → No. 9 → No. 3 → No. 1), although the direction A has more availability. Unlike the reactions of V and  $C_i$  ( $C_i-O_i$ ), V remains without interacting with the  $C_i$  of the  $C_i-C_s$  defect. This is contrary to the expectation that V and  $C_i$  would disappear, which is a remarkable point to be found by simulation.

### 3.3.8. Reaction of P and $C_i-C_s$

**Figure 14(a)** shows the calculated dependence of  $E_b$  on the number of P sites from the  $C_i-C_s$  pair. The most stable structure determined and some metastable structures are shown in Figure 14(b). Stable P– $C_iC_s$  pairs are composed of P existing at the zigzag bond in the direction B of the  $C_i-C_s$  defect. From Figure 14(a), the value of  $E_b$  is

positive even at the site with the least energy in this cell. This result indicates that the P and  $C_i-C_s$  are attracted over a distance. Figure 14(c) shows the effective charge of the  $C_i-C_s$  defect, which is negatively charged. Since P is a donor atom and positively charged, electrical interaction of P and  $C_iC_s$  pair is considered.

### 3.4. Summary of Calculations and Candidates to Affect Controllability of Lifetime

**Figure 15** shows the atomic configuration of most stable complexes formed in each reaction. The calculated results can be summarized as follows:

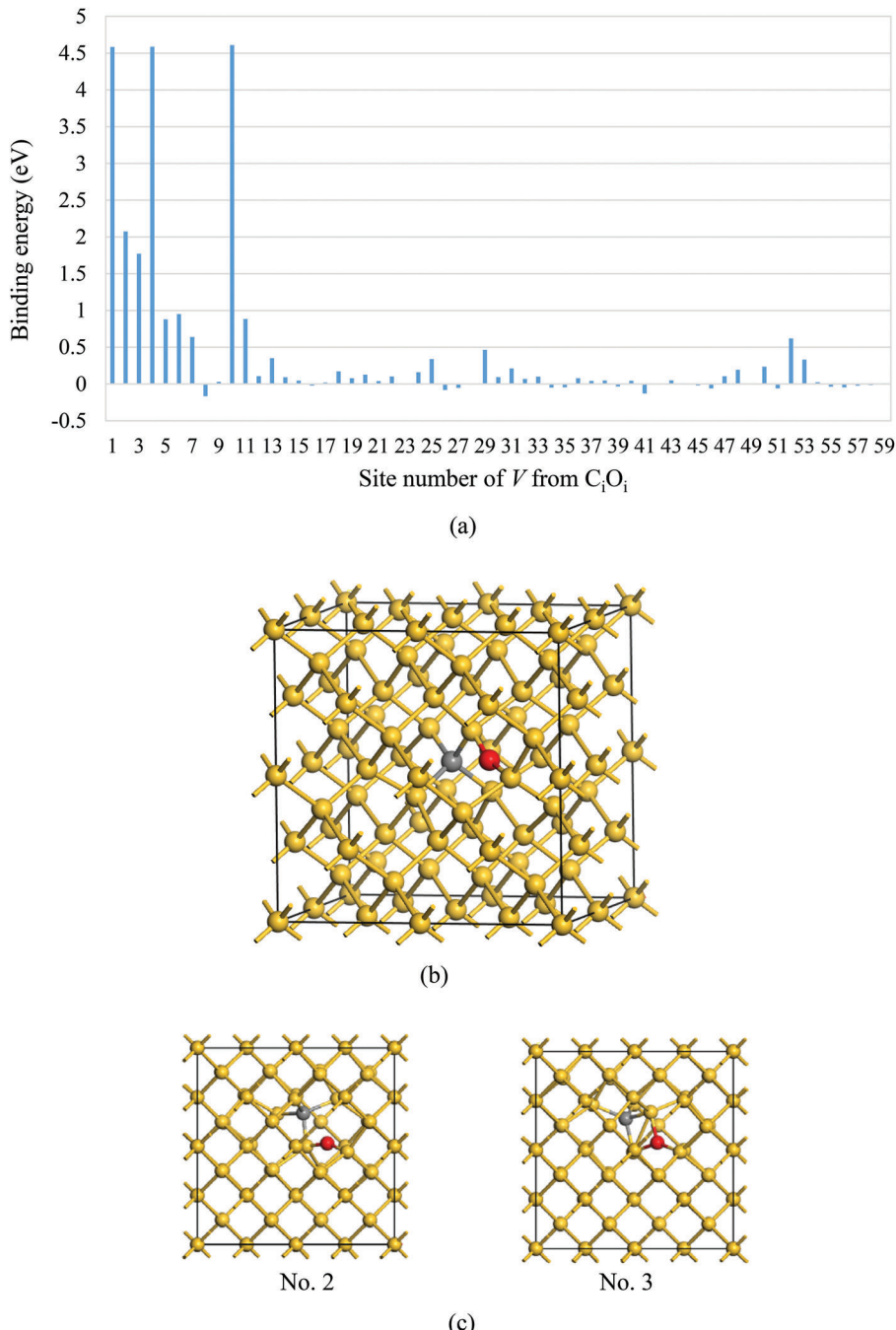


**Figure 11.** Calculation results about reaction of  $V$  and  $C_iO_i$ . a) Dependence of  $E_b$  on the number of  $V$  sites from the  $C_iO_i$  pair; b) most stable structure (No. 1, No. 4, and No. 10) (gray/red sphere indicates C/O atom); and c) metastable structures.

- 1) Lifetime-control defects ( $V-V$  and  $V-P$ )
  - i)  $V+V$ : The  $V-V$  pair is the most stable, and their interaction stays in the 1st neighbor site.
  - ii)  $V+P$ : The  $V-P$  pair is the most stable, and their interaction is beyond the cell size of Si 64-atoms.
- 2) Complexes believed to interact with lifetime-control defects
  - i)  $C_s+I$ :  $C_s-I$  forms [100] dumbbell, which is the most stable.
  - ii)  $C_i+O_i$ :  $C_i$  and  $O_i$  atoms approach each other in the direction A and form the stable rhombic structure.
  - iii)  $C_i+C_s$ :  $C_i$  and  $C_s$  atoms form [100] dumbbell, which is the most stable.
- 3) Structural change of lifetime-control defects

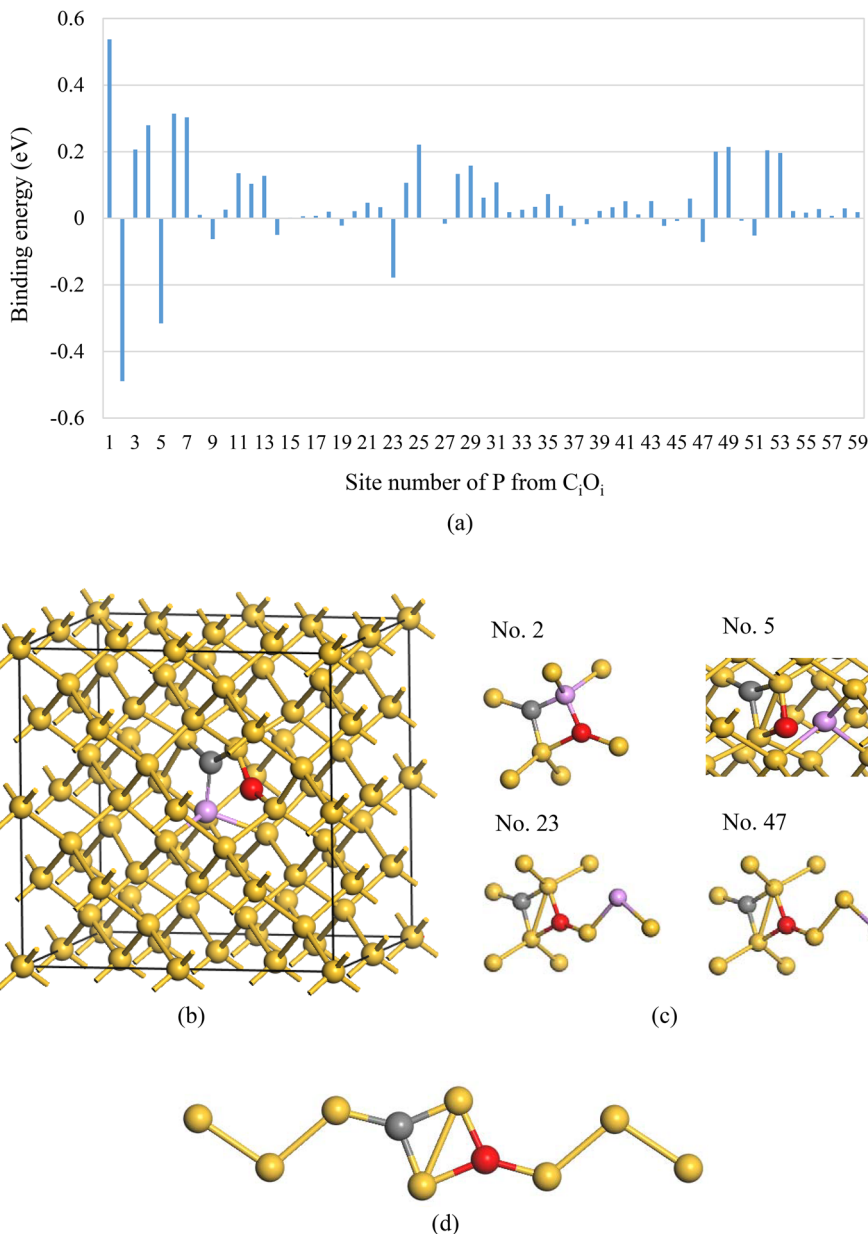


**Figure 12.** Calculation results about reaction of P and  $C_iO_i$ . a) Dependence of  $E_b$  on the number of P sites from the  $C_iO_i$  pair; b) most stable structure (No. 1) (gray/red/purple sphere indicates C/O/P atom); c) unstable structure; and d) zigzag bond including  $C_iO_i$  (a P atom is at one of the substitutional sites).

- i)  $V + C_i$ : V and  $C_i$  atoms are annihilated and a  $C_s$  atom is formed.
- ii)  $P + C_i$ : P and  $C_i$  atoms form a  $P-C_i$  dumbbell complex.
- iii)  $V + O_i$ : A  $V-O$  complex is formed by an  $O_i$  atom binding two dangling bonds of V.
- iv)  $P + O_i$ : P and  $O_i$  atoms do not bind directly.
- v)  $V + C_iO_i$ :  $C_i$  of  $C_iO_i$  interacts with V, and  $C_iO_i$  decomposes into  $C_s$  and  $O_i$  atoms.
- vi)  $P + C_iO_i$ :  $C_i$  of  $C_iO_i$  interacts with P, and  $P-C_iO_i$  decomposes into  $P-C_i$  and  $O_i$  atoms.
- vii)  $V + C_iC_s$ : V remains at the 1st nearest neighbor of  $C_i-C_s$ .
- viii)  $P + C_iC_s$ : P remains at the 2nd nearest neighbor of  $C_i-C_s$ .

**Table 2** summarizes the  $E_b$  of the most stable structures calculated by Si 64-atom and 216-atom cubic cells.  $E_b$  obtained by the previous studies are also summarized.<sup>[4,7,11,12,22–30,41]</sup> It is found that, for (i)  $C_s + I \rightarrow C_i$ , (ii)  $V + V \rightarrow V - V$ , (iii)  $C_i + O_i \rightarrow C_i - O$ , (iv)  $V + O_i \rightarrow V - O_i$ , (v)  $C_i + C_s \rightarrow C_i - C_s$ , (vi)  $P + V \rightarrow V - P$ , (vii)  $P + C_i \rightarrow P - C_i$ , the calculated  $E_b$  well agreed with that obtained in the previous studies in the range of 0.3 eV. Referring to the  $E_b$  of Fe and B ( $E_b = 0.68$  eV), which is often used for the critical value of effective gettering, the reactions above the bold line in Table 2 are likely to occur. In comparison with V and P, which are components of lifetime-control defects, the  $E_b$  of V with  $C_i$ ,  $O_i$ ,  $C_i-C_s$ , and  $C_i-O_i$  is relatively larger than that of P.

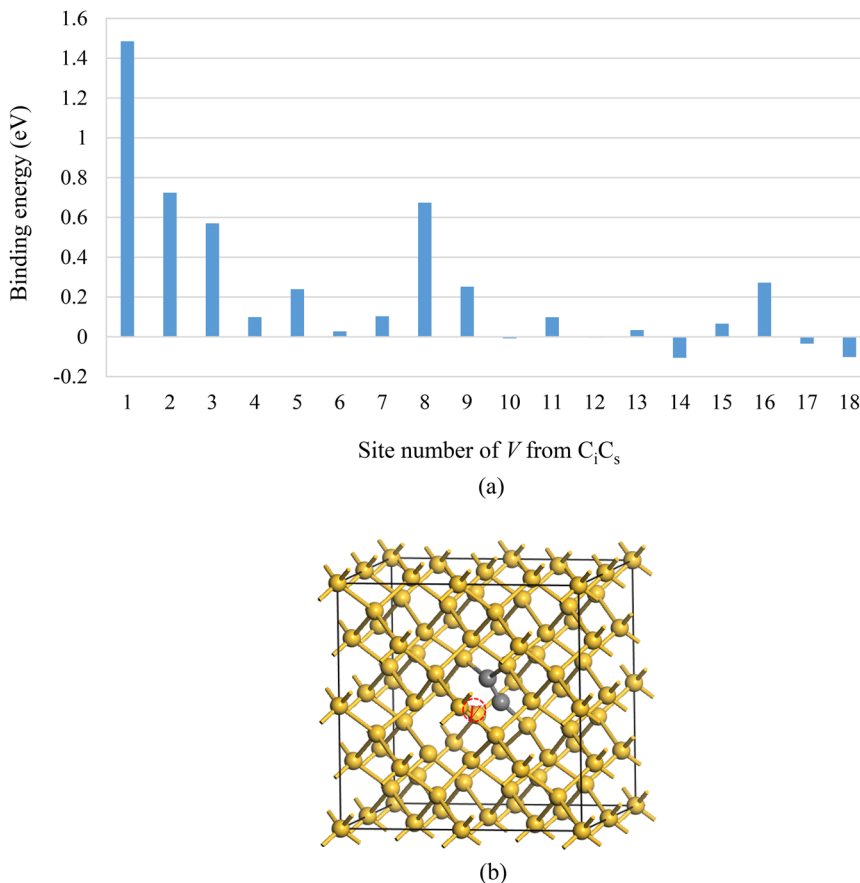


**Figure 13.** Calculation results about the reaction of  $V$  and  $C_i-C_s$ . a) Dependence of  $E_b$  on the number of  $V$  sites from the  $C_iC_s$  pair and b) most stable structure (No. 1) (gray sphere indicates  $C$  atom).

**Table 2.** Calculated  $E_b$  of most stable structures in Si 64- and Si 216-atom cubic cells.

Reaction	$E_b$ [Si 64]	$E_b$ [Si 216]	$E_b$ [previous studies]
$V + C_i \rightarrow C_s$	5.44	5.58	
$V + C_i - O_i \rightarrow C_s + O_i$	4.58	4.68	
$C_s + I \rightarrow C_i$ ( $C_s - I$ )	1.61	1.42	Cal) 1.3 <sup>[12]</sup> , 1.5 <sup>[26]</sup> , 1.56 <sup>[24]</sup>
$V + V \rightarrow V - V$	1.52	1.81	Cal) 1.43 <sup>[7]</sup> , 1.75 <sup>[22]</sup> Exp) 1.5 <sup>[4,41]</sup>
$C_i + O_i \rightarrow C_i - O_i$	1.49	1.32	Cal) 1.7 <sup>[11]</sup>
$V + C_i - C_s \rightarrow V - C_i C_s$	1.48	1.16	
$V + O_i \rightarrow V - O_i$	1.45	1.57	Cal) 1.29 <sup>[27]</sup> , 1.48 <sup>[28]</sup> , 1.50 <sup>[29]</sup> , 1.70 <sup>[30]</sup>
$C_i + C_s \rightarrow C_i - C_s$	1.36	1.03	Cal) 1.45 <sup>[23]</sup>
$P + V \rightarrow V - P$	1.02	1.18	Cal) 1.01 <sup>[23]</sup> , 1.1 <sup>[12]</sup> , 1.2 <sup>[24,25]</sup>
$P + C_i \rightarrow P - C_i$	0.88	0.82	Cal) 0.93 <sup>[23]</sup>
$P + C_i - C_s \rightarrow P - C_i C_s$	0.73	0.58	
$P + C_i O_i \rightarrow P - C_i + O_i$	0.53	0.51	
$P + O_i \rightarrow P - O_i$	0.27	0.21	

$E_b$  obtained by previous studies are also summarized.

Unit: eV.

$E_b$  of Fe and B: 0.68 eV

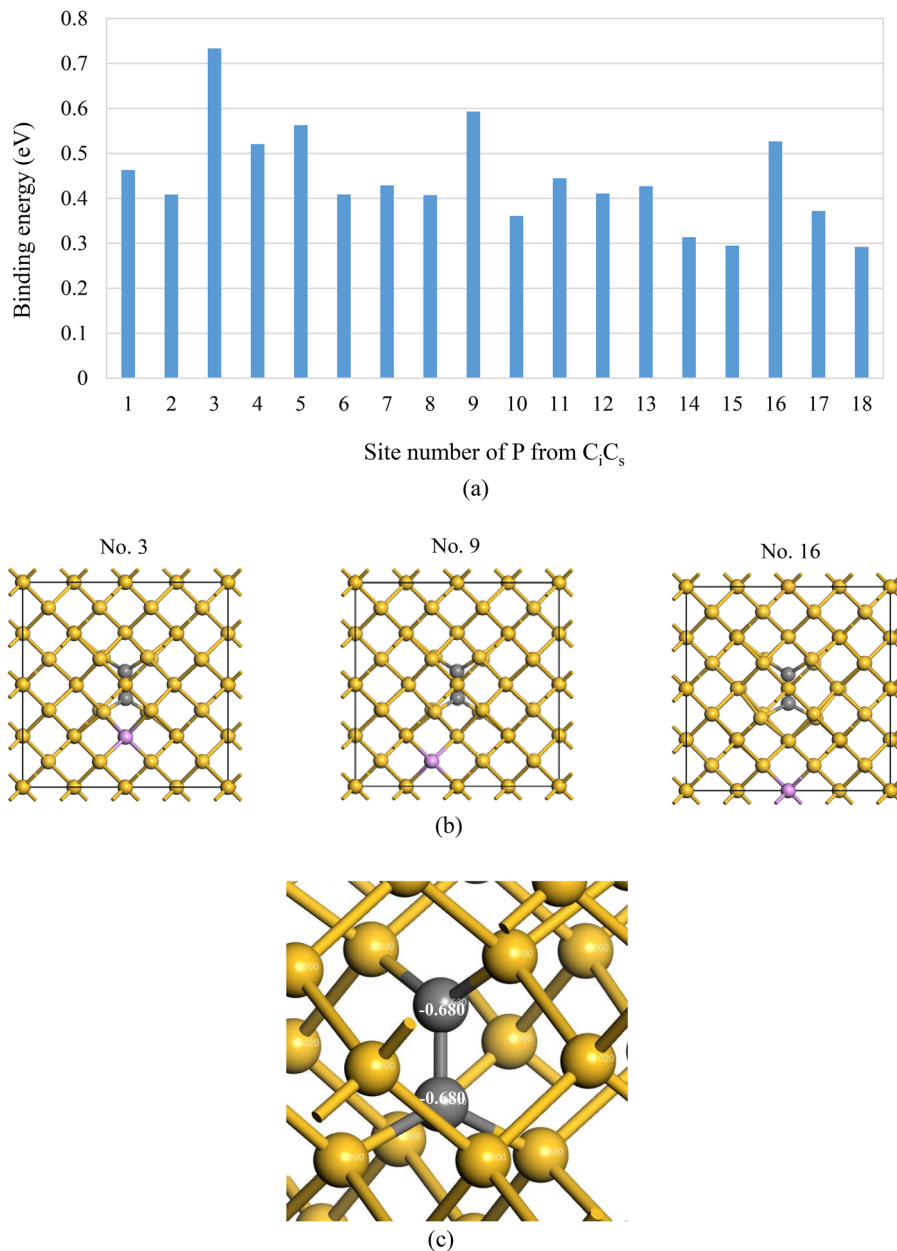


**Figure 14.** Calculation results about the reaction of P and  $C_i-C_s$ . a) Dependence of  $E_b$  on the number of P sites from the  $C_iC_s$  pair; b) most stable and metastable structures (gray/purple sphere indicates C/P atom); and c) effective charge of  $C_i-C_s$ .

Furthermore, it is found that not the  $C_i-C_s$  pair but the  $C_i$  atom and the  $C_i-O_i$  pair are the strong candidates to affect controllability of lifetime by interacting with V composed of lifetime-control defects. That is, the disappearance of deep levels of lifetime-control defects will extend the carrier lifetime by using the reaction of  $V+C_i \rightarrow C_s$  and  $V+C_iO_i \rightarrow C_s+O_i$  (independent  $C_s$  and  $O_i$  atoms do not form deep levels). The  $E_b$  of these reactions is very large so these reactions are likely to occur. This conclusion improves our understandings of the reactions that effect lifetime limiting defects.

The interactions of V-V (V-P) with  $C_i$  and  $C_i-O_i$  must be studied with a focus on the change of deep levels of lifetime-control defects in the near future.

#### 4. Conclusion

To understand the in-activation of deep energy levels of lifetime-control defects (V-V pair and V-P pair) in P doped n-type Si crystals for IGBT, DFT calculations were performed to the following behaviors related to the lifetime-control defects:

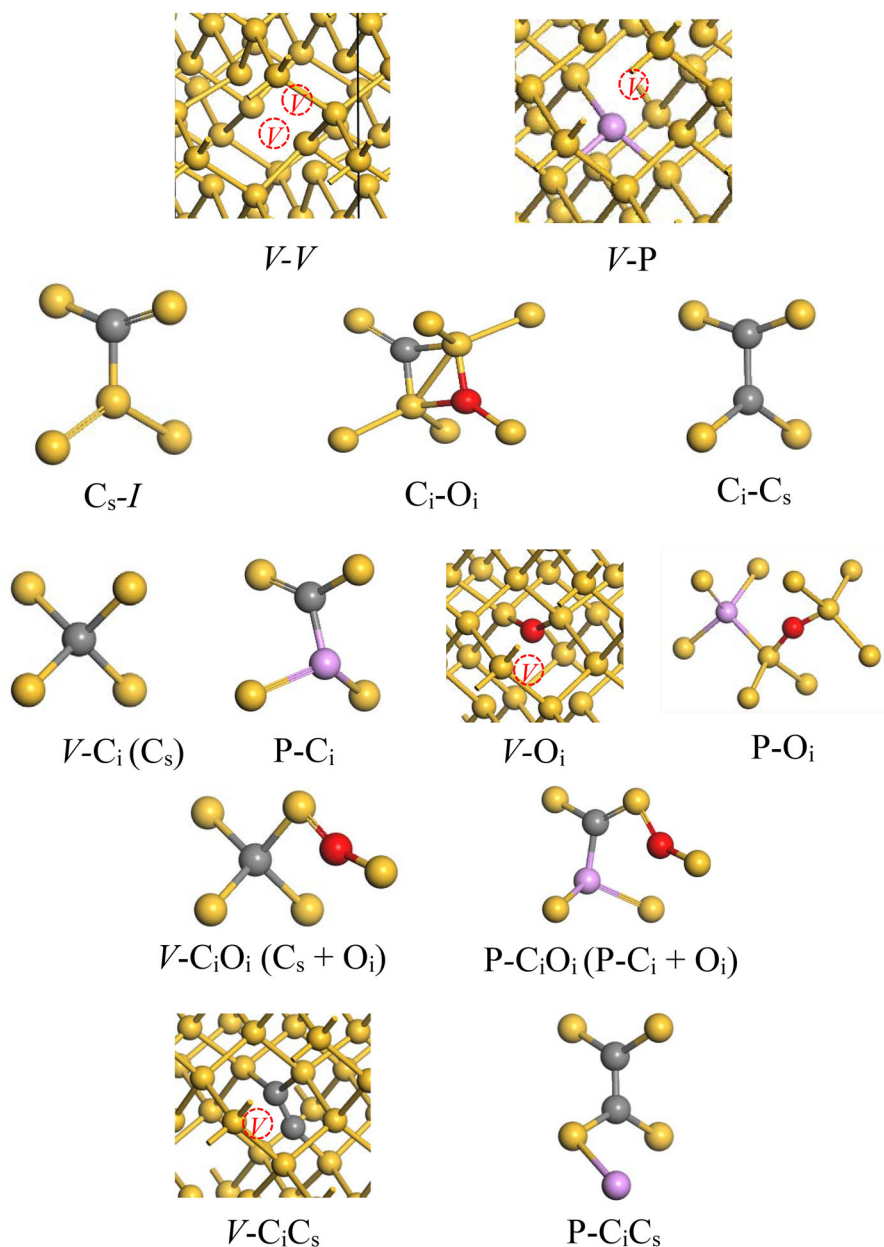


**Figure 15.** Most stable structures formed in each reaction.

- 1) Formation behavior of lifetime-control defects such as V–V and V–P.
- 2) Formation behavior of complexes ( $C_s + I$ ,  $C_i + O_i$ ,  $C_i + C_s$ ) believed to interact with lifetime-control defects.
- 3) Structural change of lifetime-control defects ( $P + C_i$ ,  $P + O_i$ ,  $V + C_i$ ,  $V + O_i$ ,  $P + C_iO_i$ ,  $P + C_iC_s$ ,  $V + C_iO_i$ ,  $V + C_iC_s$ ).

The main results are summarized in Figure 15 and Table 2. Comparing  $V$  and  $P$ , which are components of lifetime-control defects, the  $E_b$  of  $V$  with  $C_i$ ,  $O_i$ ,  $C_i-C_s$ , and  $C_i-O_i$  is relatively larger than that of  $P$ . Furthermore, instead of the  $C_i-C_s$  pair,  $C_i$  and  $C_i-O_i$  pair are strong candidates to affect the controllability

of lifetime by interacting with  $V$  composed of lifetime-control defects. That is, the disappearance of deep levels of lifetime-control defects will extend the carrier lifetime by using the reaction of  $V + C_i \rightarrow C_s$  and  $V + C_iO_i \rightarrow C_s + O_i$ .

### Acknowledgments

This work was partially supported by JSPS KAKENHI grant Number 16K04950.

### Conflict of Interest

The authors declare no conflict of interest.

**Keywords**

density functional theory, lifetime-control defect, power device, silicon crystals

Received: July 31, 2018  
Revised: December 26, 2018  
Published online:

- [1] T. Minato, K. Takano, A. Kiyo, in Proceedings of 29th International Conference on Defects in Semiconductors (ICDS) **2017**, TuA2-11.
- [2] T. Sugiyama, M. Yamazaki, A. Tanida, F. Niwa, T. Kanata, in Proceedings of the Forum on the Science and Technology of Silicon Materials **2010**, 206 and references therein.
- [3] G. D. Watkins, J. W. Corbett, *Phys. Rev.* **1964**, 134, A1359.
- [4] G. D. Watkins, J. W. Corbett, *Phys. Rev.* **1965**, 138, A543.
- [5] K. Sueoka, E. Kamiyama, J. Vanhellemont, *J. Appl. Phys.* **2013**, 114, 153510 and references therein.
- [6] N. Ganagona, L. Vines, E. V. Monakhov, B. G. Svensson, *J. Appl. Phys.* **2014**, 115, 034514.
- [7] E. Kamiyama, K. Sueoka, J. Vanhellemont, *Phys. Stat. Sol. B* **2014**, 251, 2185.
- [8] L. F. Makarenko, F. P. Korshunov, S. B. Lastovski, L. I. Murin, M. Moll, *Solid State Phenomena* **2010**, 156, 155.
- [9] M. T. Asom, J. L. Benton, R. Sauer, L. C. Kimerling, *Appl. Phys. Lett.* **1987**, 51, 256.
- [10] L. W. Song, X. D. Zhan, B. W. Benson, G. D. Watkins, *Phys. Rev. B* **1990**, 42, 5765.
- [11] L. I. Khirunenko, M. G. Sosnin, Yu. V. Pomozov, L. I. Murin, V. P. Markevich, A. R. Peaker, L. M. Almeida, J. Coutinho, V. J. B. Torres, *Phys. Rev. B* **2008**, 78, 155203.
- [12] K. Sueoka, E. Kamiyama, P. Śpiewak, J. Vanhellemont, *ECS J. Solid State Sci. Tech.* **2016**, 5, P3176.
- [13] H. Wang, A. Chroneos, D. Hall, E. N. Sgourou, U. Schwingenschlögl, *J. Mater. Chem A* **2013**, 1, 11384.
- [14] A. Chroneos, C. A. Londos, *J. Appl. Phys.* **2010**, 107, 093518.
- [15] H. Wang, A. Chroneos, C. A. Londos, E. N. Sgourou, U. Schwingenschlögl, *Appl. Phys. Lett.* **2013**, 103, 052101.
- [16] H. Wang, A. Chroneos, C. A. Londos, E. N. Sgourou, U. Schwingenschlögl, *Sci. Rep.* **2014**, 4, 4909.
- [17] A. Chroneos, E. N. Sgourou, C. A. Londos, U. Schwingenschlögl, *Appl. Phys. Rev.* **2015**, 2, 021306.
- [18] K. Kobayashi, S. Yamaoka, K. Sueoka, *J. Cryst. Growth* **2017**, 474, 110.
- [19] H. Koyama, K. Sueoka, *J. Cryst. Growth* **2017**, 463, 110.
- [20] K. Sueoka, K. Nakamura, J. Vanhellemont, *J. Cryst. Growth* **2017**, 474, 89.
- [21] F. Zirkelbach, B. Stritzker, K. Nordlund, J. K. N. Lindner, W. G. Schmidt, E. Rauls, *Phys. Rev. B* **2011**, 84, 064126.
- [22] E. Kamiyama, J. Vanhellemont, K. Sueoka, *AIP Adv.* **2015**, 5, 017127.
- [23] S. Shirawawa, K. Sueoka, T. Yamaguchi, K. Maekawa, *Mater. Sci. in Semiconductor Proc.* **2016**, 44, 13.
- [24] B. Sahli, K. Vollenweider, W. Fichner, *Phys. Rev. B* **2009**, 80, 075208.
- [25] H. Bracht, A. Croneos, *J. Appl. Phys.* **2008**, 104, 076108.
- [26] J. Zhu, T. Diaz de la Rubia, C. Mailhot, *Mater. Res. Soc. Symp. Proc.* **1997**, 439, 59.
- [27] K. Sueoka, *ECS Trans.* **2006**, 3, 71.
- [28] G. Kissinger, J. Dabrowski, D. Kot, V. Akhmetov, A. Sattler, W. Von Ammon, *J. Electrochem. Soc.* **2011**, 158, H343.
- [29] V. J. B. Torres, J. Coutinho, R. Jones, M. Barroso, S. Öberg, P. R. Briddon, *Phys. B* **2006**, 376, 109.
- [30] R. A. Casali, H. Rücker, M. Methfessel, *Appl. Phys. Lett.* **2001**, 78, 913.
- [31] A. Yamada, K. Sueoka, *ECS J. Solid State Sci. Tech.* **2017**, 6, P125.
- [32] D. Vanderbilt, *Phys. Rev. B* **1990**, 41, 7892.
- [33] J. Perdew, K. Burke, M. Ernzerhof, *Phys. Rev. Lett.* **1996**, 77, 3865.
- [34] S. J. Clark, M. D. Segall, C. J. Pickard, P. J. Probert, K. Refson, M. C. Payne, *Z. Kristallogr.* **2005**, 220, 567.
- [35] G. Kresse, J. Furthmüller, *Phys. Rev. B* **1996**, 54, 11169.
- [36] T. Fischer, J. Almlöf, *J. Phys. Chem.* **1992**, 96, 9768.
- [37] H. Monkhorst, J. Pack, *Phys. Rev. B* **1976**, 13, 5188.
- [38] A. Chantre, L. C. Kimerling, *Appl. Phys. Lett.* **1986**, 48, 1000.
- [39] G. D. Watkins, *Defects in Semiconductors 15, Materials Science Forum* (Ed: G. Ferenczi). Trans Tech, Switzerland **1989**, Vol. 38-41, p. 39.
- [40] E. Gürer, B. W. Benson, G. D. Watkins, *Defects in Semiconductors 16, Materials Science Forum* (Eds: G. Davies, G. G. DeLeo, M. Stavola). Trans Tech, Switzerland **1992**, Vol. 83-87, p. 339.
- [41] J. W. Corbett, *Electron Radiation Damage in Semiconductors and Metals*. Academic, New York **1996**, and refs. therein.